Breathable Iron-based MIL–88 Framework as Dyes Adsorbent in Aqueous Solution

Dita Arifa Nurani , Nabila Anisa , Irena Khatrin , Yasmin Yasmin , Grandprix Thomryes Marth Kadja , Yuni Krisyuningsih Krisnandi *

Posted Date: 21 December 2023

doi: 10.20944/preprints202312.1616.v1

Keywords: Metal-Organic Framework; Fe-MOF; breathable adsorbent; dyes removal; MIL-88B(Fe)

Article

Breathable Iron-based MIL–88 Framework as Dyes Adsorbent in Aqueous Solution

Dita A. Nurani [1,2], Nabila Anisa [1,2,†], Irena Khatrin [1,2,†], Yasmine [1,2], Grandprix T. M. Kadja [3,4,5] and Yuni K. Krisnandi [1,2,*]

[1] Department of Chemistry, Faculty of Mathematics and Natural Science, Universitas Indonesia, Depok 16424, Indonesia; d.arifa@sci.ui.ac.id (D.A.N); nabilaanisaa30@gmail.com (N.A.); irena.khatrin@sci.ui.ac.id (I.K.); yasaine.general@gmail.com (Y.); yuni.krisnandi@sci.ui.ac.id (Y.K.K.)

[2] Solid Inorganic Framework Laboratory, Department of Chemistry, Faculty of Mathematics and Natural Science, Universitas Indonesia, Depok 16424, Indonesia

[3] Division of Inorganic and Physical Chemistry, Faculty of Mathematics and Natural Sciences, Institut Teknologi Bandung, Jalan Ganesha No. 10, Bandung 40132, Indonesia

[4] Center for Catalysis and Reaction Engineering, Institut Teknologi Bandung, Jalan Ganesha No. 10, Bandung 40132, Indonesia

[5] Research Center for Nanosciences and Nanotechnology, Institut Teknologi Bandung, Jalan Ganesha No. 10, Bandung 40132, Indonesia

† Both students share an equal amount of work.

* Correspondence: yuni.krisnandi@sci.ui.ac.id; Tel.: +62 812-1856-7060

Abstract: Metal-Organic Frameworks (MOFs) have been observed to exclusively eliminate dyes confined within their respective pores. In this investigation, the synthesis of a breathable MOF structure, MIL-88B(Fe), was pursued with the objective of circumventing restrictions on pore size to enhance its adsorption capabilities. The synthesis of MIL-88B(Fe) was carried out via the assisted solvothermal method at 373 K using inexpensive yet environmentally benign $FeCl_3.6H_2O$, 1,4-benzenedicarboxylic acid and DMF as metal precursor, as linker and solvent, respectively. Furthermore, MOF was subjected to extensive analytical characterization using XRD, FT-IR spectroscopy, N_2 gas sorption, TGA, and SEM. The experimental data showed that the utilization of MIL-88B(Fe) with a dose level of 5 mg for 180 mins at pH of 9 led to the highest levels of adsorption for both dyes with 162.82 mg g^{-1} for Methylene Blue (MB) and 144.65 mg g^{-1} for Rhodamine B (RhB), as a result of contrast molecular size between each dye. The Langmuir and Freundlich models demonstrate a correlation with isotherms, while the thermodynamic analysis demonstrated that MIL-88B(Fe) exhibits distinct endothermic and breathable properties. The efficacy of MIL-88B(Fe) adsorbent for MB and RhB in aqueous solutions indicated exceptional performance, stability, and noteworthy reusability performance.

Keywords: metal-organic framework; Fe-MOF; breathable adsorbent; dyes removal; MIL-88B(Fe)

1. Introduction

The residual dyes from the textile, pharmaceutical, pulp, and paper industries have caused serious problems for the environment and the health of living beings due to their toxicity and carcinogenicity. In the textile industry, organic dyes are frequently used to create a variety of colors and textures. These reactive, non-degradable dyes including of methylene blue, congo red and rhodamine B often lose 10–20% of their concentration in wastewater [1,2]. A variety of methodologies has been employed for the elimination of organic dye effluent from aqueous solutions, including but not limited to chlorination, electrochemical treatment, photodegradation, coagulation, and adsorption [3–7]. Among the various techniques available for the elimination of organic colourants from large-scale aqueous environments, adsorption using a range of adsorbent materials is highly regarded due to its numerous advantages. These benefits include facile of preparation and operation, high economic value, remarkable efficiency, and suitability for a wide range of dyes. Studies imply that adsorption using diverse adsorbents work as an alternative for the elimination of organic colourants from large water bodies [8–10]. Materials such as zeolites, activated carbons and Metal

 doi:10.20944/preprints202312.1616.v1

Organic Frameworks (MOFs) have demonstrated their efficacy in the adsorption of both pollutants and organic dyes, as evidenced by previous studies [11–14].

Organic ligands and metal ions that play role as linkers and metal node precursors, respectively, in the synthesis of porous materials MOFs that have been employed for diverse applications like catalysis, gas separation, and environmental remediation [1,15–18]. MOFs have been extensively researched owing to their exceptional features, including their outstanding surface area as a resulted of the porous features with regulated pore and huge cavity sizes orderly structured [5–8]. The features and qualities of MOFs are influenced by the framework design and various synthesis techniques. As reported by Li et al, the MIL-53 has indicated a strong adsorption capacity in the elimination of malachite green and methylene blue dyes [19]. Reactive hazardous dyes like reactive yellow 15 and red 25 have been effectively removed by MIL-101 [1]. Additionally, MIL-88NH_2 was also reported to be an effective adsorbent for removing Congo Red through chemisorption with outstanding adsorption stability and a straightforward regeneration process [20].

The thermal stability of MOFs is a consequence of the robust characteristic of the metal ions and ligands bonding interaction. Numerous metallic ions in MOFs have been investigated in relation to the adsorption and elimination of organic dyes, including Al-MOF, Zn-MOF, Cu-MOF, Cr-MOF, Y-MOF, Co-MOF, and Fe-MOF [1,21–24]. On the basis of our earlier findings, several transition metal-based MOFs have been described. For instance, high thermal stability Co-MOF and high surface area Y-MOF crystalline both demonstrated excellent performance as adsorbents for rhodamine B and methylene blue, respectively [25,26]. Transition metals have been reported to enhance the physicochemical properties of the as-synthesized MOF. However, many transitional metals, including noble metals, are relatively expensive and don't meet the requirements to be used on an industrial scale. Therefore, we are keen to report the synthesis of MOFs using abundant and inexpensive transition metals. The semiconductor characteristics, strong catalytic activity, and stability of iron (Fe) have generated a great deal of attention. It is also non-toxic, the cheapest, and one of the most abundant metals. The oxidation number of metal ions also contributes to the force of electrostatic attraction, which holds the whole structure of MOF together. The ligands in MOF structures are said to form strong connections with trivalent metal ions [27]. In a prior publication, we described a single-step process for replacing the Cr^{3+} ions in MIL-101 with Fe^{3+} and Sc^{3+}, which produced the polymorphic MOF MIL-88B with a somewhat low stability structure [28].

MOFs have been identified as a potential technology for dye adsorption in water treatment. However, recent studies by Uddin *et al*. have revealed that the inconsistent and stable trait of the pore size in MOFs presents a significant obstacle to the efficient utilization of MOFs in this context [21]. MOFs typically only apply to dyes with particle size smaller than the MOF's pore size and volume. Large-particle dyes cannot be effectively removed from aqueous solutions by MOFs with relatively low pore sizes, while MOFs with large pore sizes aren't selective enough to remove small-particle dyes from aqueous solutions. Numerous MOFs have been thoroughly developed with flexible and dynamic features in an effort to enhance their potential applications. The one-dimensional channels as a building block of MOF may reversibly lengthen or shorten depending on thermodynamic variables like temperature, pressure, or trapped molecules [29,30]. Volringer *et al.* and Chaplais *et al.* described that the flexibility feature known as the breathing effect, is dependent on the metal center of MOFs [31,32]. For instance, MIL-53(M) MOFs, denoted by *M* as metal such as Al, Ga, Fe, Cr, Sc and In, can breathe due to their flexible diamond-shaped scaffolds [29]. Meanwhile, Surblé *et al.* developed a series of MIL-88 metal-organic frameworks that consist of hexagonal 6-connected breathable network structures [33].

This work involved the replacement of Cr^{3+} in MIL-101 with inexpensive and environmentally benign Fe^{3+}, which produced MIL-88B(Fe). Eco-friendly metal Fe and BDC ligands were used in a one-step solvothermal synthesis process with DMF. The MIL-88B(Fe) material then was subsequently employed as an adsorbent to eliminate dyes from aqueous solutions. Cationic dyes with differences in particle size, including MB (methylene blue) and RhB (rhodamine B), larger molecular-size dyes as depicted in Figure 1, were employed as model compounds to signify the flexibility properties of as-synthesized MOF. The optimal adsorption environments, including of initial dyes dose, contact

Preprints (www.preprints.org) | NOT PEER-REVIEWED | Posted: 21 December 2023 doi:10.20944/preprints202312.1616.v1

time, pH, as well as adsorption-related variables such as isotherms, kinetics, and thermodynamics, were investigated. Furthermore, the reusability and selectivity against two cationic dyes of MIL-88B(Fe) was investigated.

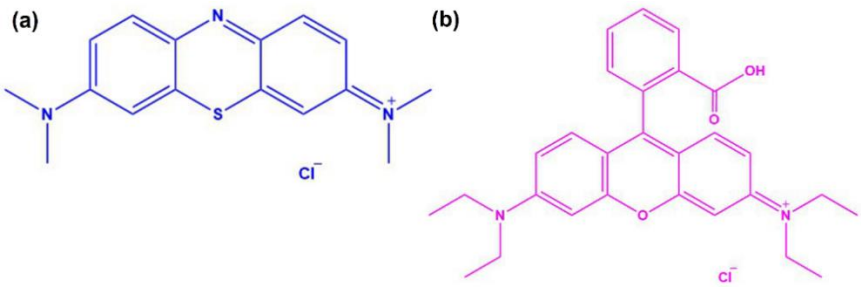

Figure 1. The chemical structure of MB (a) and RhB (b).

2. Materials and Methods

2.1. Materials

The chemicals utilized in this report, namely: Iron (III) chloride hexahydrate (pa 97%), 1.4-benzenedicarboxylic acid (pa, 98%), dimethylformamide (DMF) with purity of 99.8%, methylene blue (95%), rhodamine B (95%) percent purity, as well as sodium hydroxide (NaOH), acetic acid (CH_3COOH), and ethanol were all obtained from Sigma Aldrich. All substances were utilized in their original form without any purification. The solvent employed for the adsorption experiments was distilled water.

2.2. Synthesis of MIL-88B(Fe)

The synthesis of MIL-88B(Fe) MOF was carried out using the methodology as reported by Zhu *et al.* with some modifications [7]. A mixture of 4.9 mmol and 2.5 mmol of iron (III) chloride hexahydrate and 1,4-benzenedicarboxylic acid, respectively, was obtained by dissolving the reagents in 30 mL of dimethylformamide (DMF) with continuous stirring for 30 m. Subsequently, the mixture was crystallized for 20 h in the oven using a 50 mL-autoclave lined with Teflon at 373 K. The resultant product was subjected to two rounds of ethanol washing at 333 K for a duration of 3 h each, to eliminate any unreacted material. Subsequently, it was heated at 333 K for 24 h.

2.3. Characterization of MIL-88B(Fe)

Alpha Bruker Fourier Transform-Infra Red (FT-IR) spectrometer was performed under KBr method (4 cm^{-1} resolution) to analyze the functional groups within MOF. PANanalytical: X'Pert Pro XRD was utilized to record the XRD patterns under the radiation of Cu-Kα at 40 kV and 30 mA (λ =1.54184 Å). The surface area of MOF was evaluated using the Brunauer–Emmett–Teller (BET) method on a Surface Area Analyzer (SAA) Quantachrome-Evo Surface Area and Pore Size Analyzer with N_2 at 77 K. Whereas the t-plot method was applied to determine the external surface area and micropore volume. Total pore volume was measured from the amount of N_2 adsorbed at $P/P_0 = 0.99$. The Scanning Electron Microscope (SEM) Quanta 650 at 20 kV was applied to understand the morphologies of MOF. The Thermogravimetric Analysis (TGA) was carried out on Thermogravimetric-Differential Thermal Analysis LINSEIS STA Platinum Series instruments of 10 °C/min heating rate of N_2 flow.

2.4. Adsorption Experiments

MB and RhB as two organic cationic compounds which varied in molecular size, were chosen as the model to evaluate the efficacy and breathing impact of MIL-88B(Fe) materials. 5 mg of MIL-88B(Fe) was applied to 5 mL of 5 mg L^{-1} MB and RhB. The adsorption experiments were conducted

Preprints (www.preprints.org) | NOT PEER-REVIEWED | Posted: 21 December 2023 doi:10.20944/preprints202312.1616.v1

for 120 min at room temperature. The respective concentration of MB and RhB dyes was then ascertained by an ultraviolet-visible (UV-Vis) spectrophotometer (T92+, PG Instruments) at λ_{max} = 554 and 664 nm. The adsorption capacity at a certain time (q_t, mg g^{-1}) and equilibrium (q_e, mg g^{-1}) was determined from the equation:

$$q_t = \frac{(C_0 - C_t)V}{m} \quad (1)$$

$$q_e = \frac{(C_0 - C_e)V}{m} \quad (2)$$

where C_0, C_t, and C_e are the initial dye concentrations (mg L^{-1}), at equilibrium, and certain time t, respectively. m is described as the adsorbent mass (g) and V is the volume of dye solution (L).

3. Results and Discussion

3.1. Synthesis and Characterization of MIL-88B(Fe)

Figure 2a depicts the XRD pattern of the as-resulted MIL-88B(Fe). According to the study by Zhu *et al.*, on their synthesis of MIL-101(Fe) which method was followed with modification in this paper, it was stated that MIL-101 possesses characteristic diffraction peaks at 2θ = 3.3°, 6.9°, and 7.3° (CCDC No. 605510) [7]. Whereas the as-synthesized MOF XRD pattern exhibits diffraction peaks at 2θ = 9.0°, 9.7°, 10.0°, 16.5°, and 16.8°, some new phases also appeared at 2θ = 9.4°, 12.5°, and 18.6° corresponding to MIL-88B, which is the framework isomer of MIL-101 [28]. The Rietveld refinement approach was carried out to the reference (CCDC No. 1892483) and experimental XRD patterns of MIL-88B based on the triclinic structure with P-1 space group (Figure S1) revealing the goodness of fit (defined by $G = \chi^2$) at 1.068. These results indicate the effective creation of MIL-88B(Fe) which is supported by a well-fitted diffraction of the reference and experimental data [1,34]. The modifications to the synthesis technique, such as raising the temperature, extending the reaction time and alteration on the ratio of the precursors in comparison to MIL-101, may have an impact on these alterations in the framework structure [35].

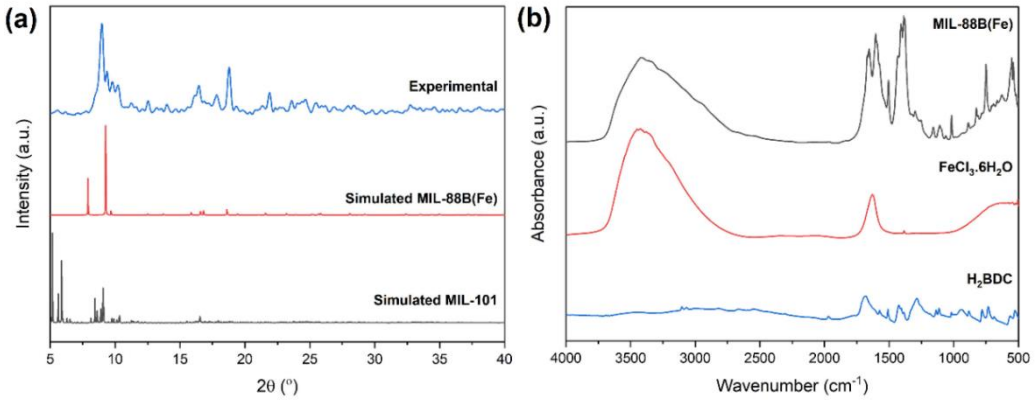

Figure 2. XRD patterns (a) and FT-IR spectra (b) of MIL-88B(Fe).

Figure 2b presents the FT-IR spectra of as-resulted MOF, $FeCl_3.6H_2O$ as the metal precursor, and 1,4-benzenedicarboxylic acid as the linker. The MOF exhibits absorption peaks at 3520 and 2950–2935 cm^{-1} relating to the functional group of O–H stretching, C–H sp^2, respectively. While adsorption peaks at 1672 and 1380–1450 cm^{-1} both corresponding to C–H bending. Furthermore, absorption peaks observed at 600–500 cm^{-1} owned by Fe–O band vibrations with metal precursors. A slight shift of C=O peaks of the organic linker, both asymmetric and symmetric vibrations, to the lower wavenumber at 1672 cm^{-1} indicated the bond between linker and metal of MIL-88(Fe) confirming the XRD results.

Preprints (www.preprints.org) | NOT PEER-REVIEWED | Posted: 21 December 2023 doi:10.20944/preprints202312.1616.v1

According to the SEM analysis of MIL-88B(Fe), it exhibits an octahedral structure (Figure. 3a–b) similar to that of a conventional crystalline and porous Fe-based MOF reported by Zhu, T. *et al.* and Taylor-Pashow *et al.* [7,15,36]. The EDX spectrum of MIL-88B(Fe) (Figure. S2) reveals the existence peaks of C, O, Fe and Cl elements which also are detailed in Table 1. Moreover, the SEM elemental mapping images (Figure. 3c) confirm the homogeneous dispersion of each element in MIL-88B(Fe). Figure S3 illustrated the N_2 physisorption isotherm and BJH pore size distribution of the as-resulted MIL-88B(Fe) which show a significant H-4 hysteresis loop of material with the distinct mesoporous structure with surface area of 275.12 $m^2\ g^{-1}$, pore volume of 0.078 $cm^3\ g^{-1}$ and an average pore diameter of 6.2 nm (Table 1).

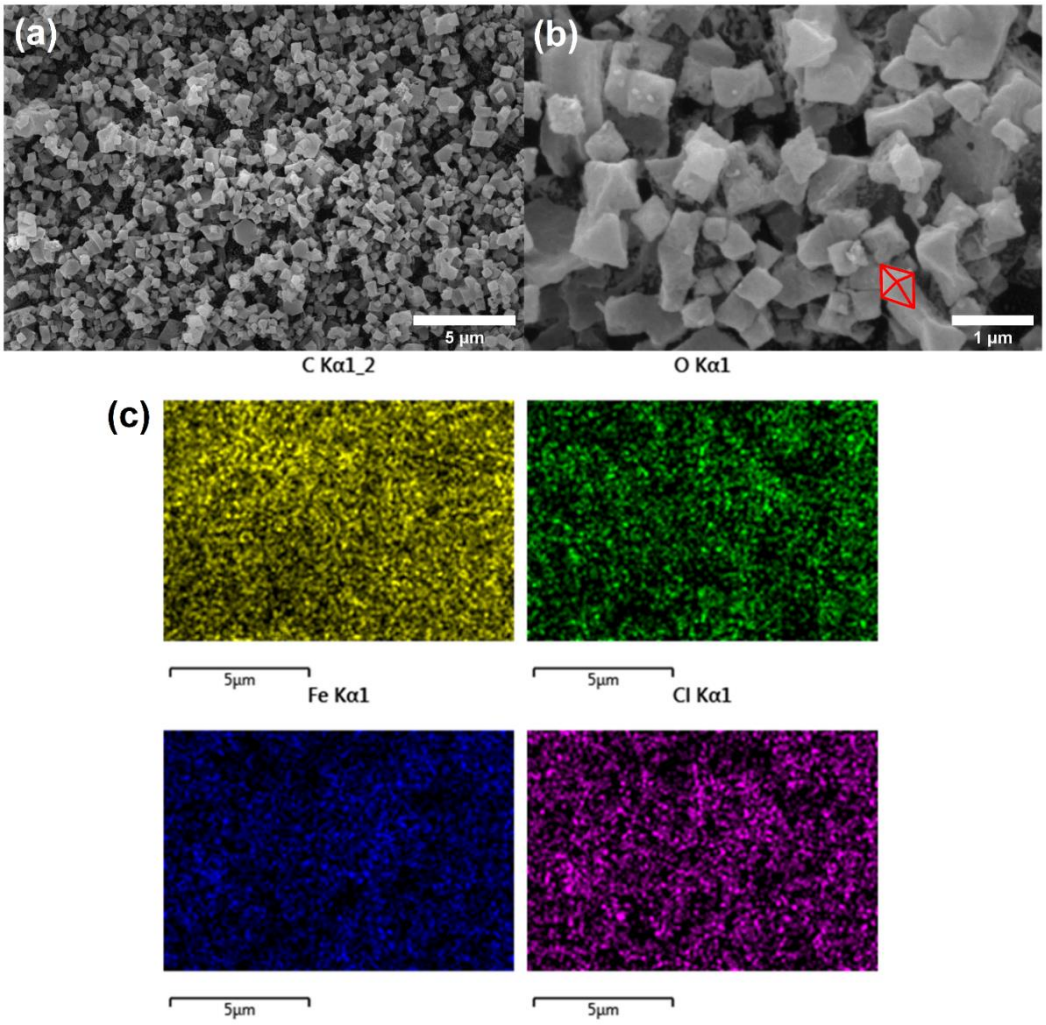

Figure 3. SEM images (a-b) and corresponding elemental mapping images (c) of MIL-88B(Fe).

Table 1. Physicochemical properties of MIL-88B(Fe).

S_{BET} ($m^2\ g^{-1}$) [a]	V_{Total} ($cm^3\ g^{-1}$) [b]	Avg. Pore Diameter [c]	% Wt. [d]			
			C	O	Fe	Cl
275.12	0.078	6.20	61.8	25.4	10.8	2.0

[a] Determined using BET method.

[b] Determined at $p/p_0 = 0.99$.

[c] Determined using BJH method.

[d] Determined using EDX.

MIL-88B(Fe) was evaluated for thermal stability using TGA from 25 °C to 750 °C (Figure 4). Five plateaus were detected in the TG curve. 16.9% of weight loss at 90–120 °C resembles the evaporation

Preprints (www.preprints.org) | NOT PEER-REVIEWED | Posted: 21 December 2023 doi:10.20944/preprints202312.1616.v1

of H2O molecules, while the second plateau, which occurs between 300 and 700 °C linked to the breakdown of an organic framework with the mass loss of 40% corresponds to two BDC linkers used in the synthesis, which leads to the fabrication of iron oxide at 750 °C. The mass reduction is in agreement with the original formula of crystal as [$Fe_3O(OH)(BDC)_3(H2O)_2$], which is consistent with earlier findings by [11]. DTA analysis in Figure 4 reveals an endothermic peak below 120 °C with minor weight loss. The significant weight loss corresponds well with the DTA results by the appearance of two exothermic peaks at around 360 °C and 680 °C as resulted by the loss of organic fragments and confirm the stability of MIL-88B(Fe) until 300 °C.

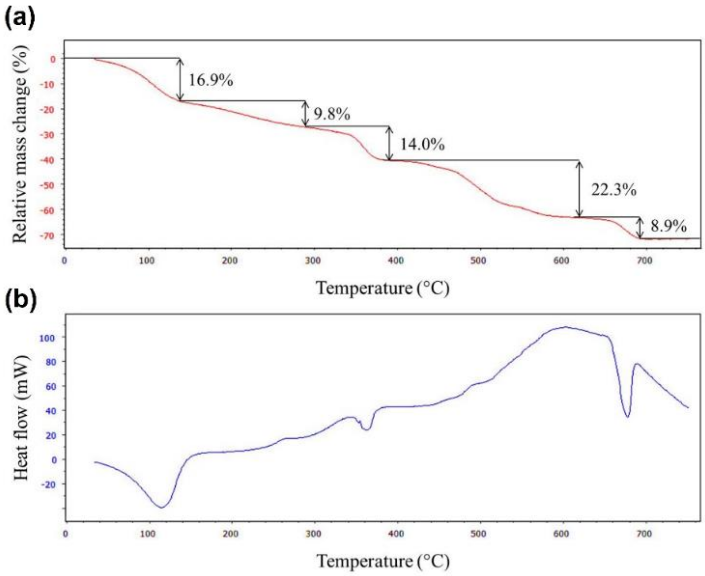

Figure 4. Thermogravimetry/differential thermal analysis (TGA/DTA) profile of MIL-88B(Fe).

3.2. Adsorption Experiments

3.2.1. Effect of pH

The impact of initial pH on the MIL-88B(Fe) adsorption of MB and RhB was investigated in the pH range of 3 to 12. The findings are presented in Figure 5a. The adsorption capacity of MIL-88B(Fe) towards MB and RhB increased gradually when the pH was altered from 3 to 9 and decreased at pH 12. The optimum adsorption capacity of MIL-88(Fe) was observed at pH 9. This could be due to the electrostatic interaction that regulates the adsorption of MB and RhB. The positive charge density of MIL-88B(Fe) increased at an acidic pH, which reduced the adsorption of cationic dyes as explained by electrostatic repulsion. In addition, excess H^+ ions in the solution were observed to compete with cationic dyes for the active sites of MIL-88B(Fe) causing a decrease in adsorbed dyes [19]. On the opposite, at pH 9, the negative charge density of MOF expanded due to the deposition of OH- ion on the MIL-88B(Fe) surface. It showed high adsorption capacity to the positively charged cationic dyes through electrostatic interaction. At a basic pH, the hydroxyl groups (O-H) and carbonyl groups (C=O) on the external area of the MOF attracted the cationic dye compounds [37]. Furthermore, at pH > 9, the adsorption capacity decreased significantly. Previous research also reported that the optimum pH of Co-MOF and Fe-MOF with the succinic acid linker to absorb MB is pH 9 [26]. This condition was necessary because MIL-88B(Fe)'s structure might disintegrate and begin to hydrolyze in a strongly basic solution. [19].

Preprints (www.preprints.org) | NOT PEER-REVIEWED | Posted: 21 December 2023 doi:10.20944/preprints202312.1616.v1

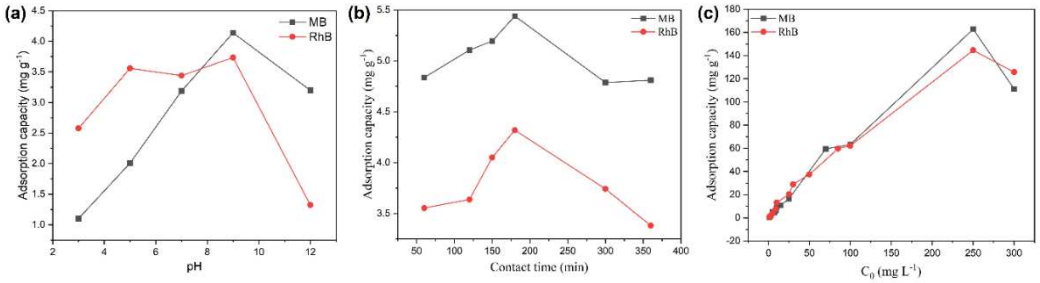

Figure 5. The effect of pH (a), contact time (b), and initial dye concentration (c) on the adsorption capacity of MIL-88B(Fe) towards MB and RhB.

3.2.2. Effect of Contact Time

Figure 5b demonstrated the impact of contact time to the adsorption of dyes by MIL-88B(Fe), which was examined at 60 to 360 min time intervals at pH 9. The adsorption profile was observed to be the similar for both cationic dyes and comprised of two phases. The first phase at 60–180 min owning to the adsorption of MB and RhB with the initial dose of 5 mg L^{-1} to reach the equilibrium adsorption state. The adsorption capacity, q value, expanded rapidly with extending time due to a tremendous number of active sites on the external area of MIL-88B(Fe). The second adsorption phases started once the binding between the dyes (MB and RhB) and MIL-88B(Fe) adsorbent was completed. The adsorption capabilities reduced during the 180–360 min contact time due to a weakening of the binding as the dyes increasingly saturated the MOF surface.

3.2.3. Effect of Dyes Initial Concentration

Figure 5c illustrates in incremental on the adsorption capacity of the MIL-88B(Fe) towards both MB and RhB dyes as the initial dye concentration increased and saturated at 250 mg L^{-1}. Due to a lack of active sites, an increase in dye concentration would result in the reduction of dye removal [37]. According to the findings under optimum circumstances, the optimal MOF capacity on MOF on MB and RhB were 162.82 mg g^{-1} and 144.65 mg g^{-1}, respectively. This suggests that the molecular size of the dyes also affects the adsorption process. Since RhB possesses a greater molecular size (~ 1.77 nm) compared to MB (~ 1.40 nm), it might limit the penetration process of RhB into the pores on MIL-88B(Fe) surface.

3.2.4. Adsorption Isotherms

The MB and RhB adsorption isotherm on MIL-88B(Fe) under the ideal adsorption conditions of pH 9, contact period 180 min, and starting dye concentration 250 mg L-1 is depicted in Figure 6a-b. The Langmuir and Freundlich models were fitted as the typical models for liquid-phase adsorption.

$$\frac{C_e}{q_e} = \frac{1}{K_L q_{max}} + \frac{Ce}{q_{max}} \quad (3)$$

Eq. 3 represents the Langmuir isotherm equation, with Ce (mg L-1) denoting the equilibrium solute concentration, qmax denoting the maximum amount of adsorption, and KL (L mg-1) denoting the Langmuir adsorption constant related to the adsorption binding energy [19]. Adsorption is thought to be a monolayer process according to the Langmuir model. The linear fitting of Ce/qe vs. Ce (Figure 6a) may be used to determine the values of R2 and Langmuir constants (KL), where a large KL value indicates a favorable adsorption process. The adsorption isotherm constants are listed in Table 2. In contrast to RhB, MB had an R2 value of >0.99 when the Langmuir isotherm model was fitted. At concentrations between 1 and 9 ppm, qmax value of RhB was found to be higher than MB. It was observed that the qmax value of RhB was higher than the qmax of MB at the concentration range of 1 to 9 ppm. The experimental data on adsorption capacity (Figure 6a) also showed that MIL-88B(Fe) displays better RhB adsorption capacity at low concentrations.

Preprints (www.preprints.org) | NOT PEER-REVIEWED | Posted: 21 December 2023 doi:10.20944/preprints202312.1616.v1

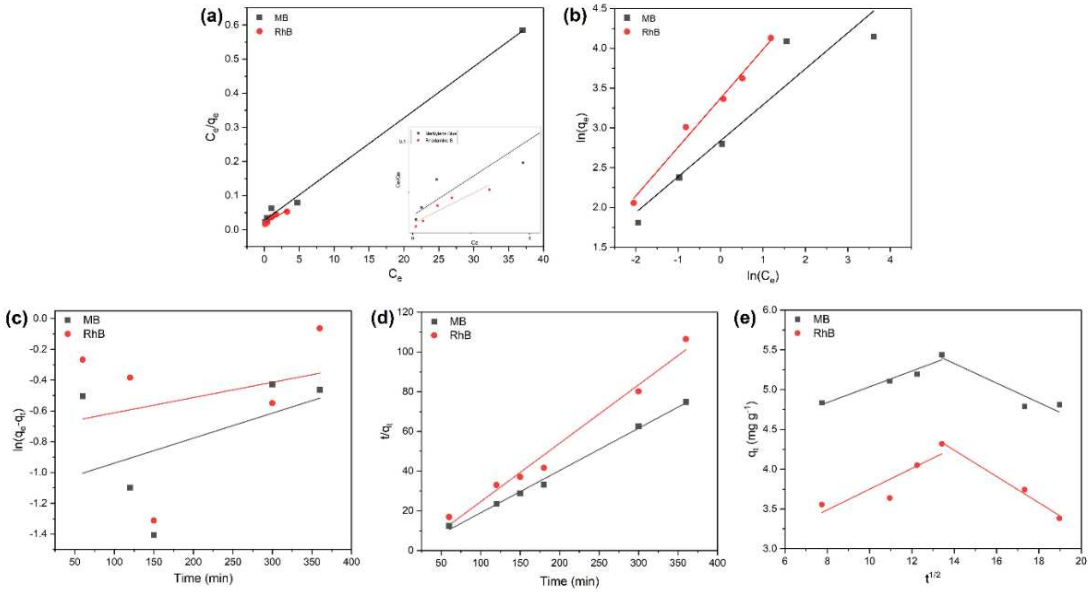

Figure 6. The linear-fitting of Langmuir (a) and Freundlich (b) isotherm model; and the linear-fitting kinetics by pseudo-first order (c), pseudo-second order (d), and intraparticle diffusion model (e) of MB and RhB.

Table 2. Langmuir and Freundlich isotherm constant of MIL-88B(Fe).

Dyes	Langmuir Model			Freundlich Model		
	q_{max} (mg g^{-1})	K_L (L mg^{-1})	R^2	$1/n$	K_F	R^2
MB	66.67	0.5555	0.9965	0.4511	17.10	0.9014
RhB	86.96	0.5928	0.8818	0.6135	29.15	0.9877

Furthermore, the adsorption isotherm results were also fitted with the Freundlich model (Figure 6b) as follows:

$$\log q_e = \log K_f + \frac{1}{n} \log C_e \quad (4)$$

where Kf is the Freundlich constant, and n is correlated with the adsorption strength [24]. The Freundlich isotherm presumptively includes both monolayer and multilayer adsorption in heterogeneous adsorption. The MB adsorption is well-fitted to the Langmuir model, as evidenced by the higher R2 value. Therefore, it is proposed that MB adsorption is confined on a monolayer and the adsorption sites are homogeneous. The adsorption of MB on the surface of Fe-MOF (succinic acid ligand) has also been studied in the past to fit the Langmuir model [26]. Whereas the Freundlich model concurs with the experimental findings on RhB adsorption. Furthermore, it is suggested that the bond between both cationic dyes and the external area of MOF-88B(Fe) is not entirely a monolayer adsorption. A small number of heterogeneous adsorptions may also exist, and the driving force may come from chemical adsorption [26].

3.2.5. Adsorption Kinetics

The adsorption process and behavior of dyes were examined by fitting the kinetic experimental data to pseudo-first-order and pseudo-second order kinetic models (Figure 6c-d) [38]. The rate constants of pseudo-first order (k_1) and pseudo-second order (k_2) may be obtained from the fitted data [39]. The pseudo-first-order kinetic model (Figure 6c) presupposes that adsorption is a diffusion-controlled process, with the adsorption rate being defined as the difference between the equilibrium and time-dependent adsorption capacities [40]. The pseudo-first-order formula is as follows:

$$\ln(q_e - q_t) = \ln q_e - k_1 t \quad (5)$$

Preprints (www.preprints.org) | NOT PEER-REVIEWED | Posted: 21 December 2023 doi:10.20944/preprints202312.1616.v1

where q_t (mg g^{-1}) is the quantity of the adsorbent that was adsorbed at time t (min) and q_e (mg g^{-1}) is the amount of adsorption that was present at equilibrium. In contrast, the pseudo-second-order model (Figure 6d) postulates that the adsorption occurs because of electron sharing or transfer between adsorbent and absorbent or is simply referred to as chemical adsorption [39]. The pseudo-second-order kinetic model formula is:

$$\frac{t}{q_t} = \frac{1}{k_2 q_e^2} - \frac{t}{q_e} \quad (6)$$

Table 3 displays the kinetic parameters as well as the correlation coefficients (R^2). The pseudo-second-order kinetic model provides the best fit for the adsorption of the dyes MB and RhB, indicating that the rate-determining step is chemisorption based on the higher correlation coefficient values of the pseudo-second order compared to the pseudo-first order and the value of the second dynamic adsorption (q_{cal}), which is not far from the experimental value (q_{exp}) [41].

The intraparticle diffusion was also studied to analyse the adsorption process by fitting the kinetics data to the formula:

$$q_t = k_i t^{\frac{1}{2}} + c \quad (7)$$

where k_i is the intramolecular diffusion constant and c (mg g^{-1}) is a constant. The multilinear graphs, as shown in Figure 6e reveal that the adsorption of MB and RhB occurred in two-step stages. The initial phase is the film diffusion model, which describes how dye molecules distribute from a mixture to the interlayered external area of the adsorbent. While the latter phase is the intraparticle diffusion phase, which is the diffusion of dyes into the porous system of the adsorbent [42,43]. The intraparticle diffusion model is suitable for the analysis of both MB and RhB adsorption on MIL-88B(Fe), and the strong correlation coefficient demonstrates that the rate-controlling step for MB and RhB is the diffusion of dyes into the adsorbent pores. [44].

Table 3. Adsorption kinetics parameters of MB and RhB adsorption.

Dyes	**Parameters**	**Dyes**	
		MB	**RhB**
Pseudo-second-order Model	q_{cal} [a] (mg g^{-1})	4.70	3.40
	q_{exp} [b] (mg g^{-1})	5.44	2.76
	k_2 (g mg^{-1} min^{-1})	1.99 x 10^{-2}	1.78 x 10^{-2}
	R^2	0.9951	0.9808
Pseudo-first-order Model	q_{cal} [a] (mg g^{-1})	0.3324	44.456
	k_1 (min^{-1})	1.6 x 10^{-3}	6.0 x 10^{-4}
	R^2	0.213	0.0971
Intraparticle Diffusion Models	k_{i1} (mg g^{-1} min$^{-1/2}$)	0.10	0.13
	C_1 (mg g^{-1})	4.04	2.44
	R^2	0.9491	0.7908
	k_{i2} (mg g^{-1} min$^{-1/2}$)	0.12	0.17
	C_2 (mg g^{-1})	7.05	6.55
	R^2	0.8981	0.9906

[a] $q_{e,exp}$ is the equilibrium adsorption capacities in accordance to the experiments.

[b] $q_{e,cal}$ is determined in accordance to the linear fitting from the kinetic models.

3.2.6. Adsorption Thermodyamics

The thermodynamic study was conducted at temperatures of 298, 308, and 318 K with the findings shown in Table 4 to further analyze the adsorption behavior of MB and RhB on MIL88(Fe). The thermodynamic parameters analysed the adsorption enthalpy change ($\Delta H°$), the Gibbs free energy change ($\Delta G°$), and the entropy ($\Delta S°$) where each is indicative of the system's heat content, the

Preprints (www.preprints.org) | NOT PEER-REVIEWED | Posted: 21 December 2023 doi:10.20944/preprints202312.1616.v1

reaction spontaneity, and the disordered degree of the adsorption process, respectively, calculated by [40]:

$$\ln\left(\frac{q_e}{C_e}\right) = -\frac{\Delta H^\circ}{RT} + \frac{\Delta S^\circ}{R} \quad (8)$$

$$\Delta G^\circ = \Delta H^\circ - T\Delta S^\circ \quad (9)$$

where the absolute temperature and the universal gas constant are donated as T (K) and R (8.314 J mol^{-1} K^{-1}), respectively. The positive value of ΔH° reveals that the adsorption process of MB and RhB is endothermic, where the performance of the adsorption is especially influenced by an elevation in temperature. The positive value of ΔS° implies an increase in entropy reduction and system chaos reduction in the adsorption processes of MB and RhB. The degree of freedom of the system was raised by the adsorption additional solute molecules [39]. Meanwhile, the ΔG° value of MB ($\Delta G^\circ < 0$) and RhB shows a little bit of difference, as RhB only possessed $\Delta G^\circ > 0$ at T = 318 K, which implies that the adsorption of MB is spontaneous even at ambient condition, unlike the adsorption of RhB that happen spontaneously at T = 318 K or higher. These results are supported by the fact that the molecular size of RhB (~1.77 nm) is larger than that of MB (~1.40 nm). However, the adsorption still happens spontaneously at T > 318 K which confirms the breathable characteristic possessed by MIL-88B(Fe) due to the flexibility of the pores (Ø6.2 nm) to expand and accommodate RhB molecules.

Table 4. Thermodynamic parameters of MB and RhB adsorption.

Dyes	T (K)	ΔG° (kJ/mol)	ΔH° (kJ/mol)	ΔS° (J/mol/K)
MB	298	–2.42	42.98	152.30
	308	–3.95		
	318	–5.47		
RhB	298	1.65	28.17	88.95
	308	0.76		
	318	–0.12		

3.2.7. Reusability

Reusability is an important factor for an effective adsorbent in large-scale applications. The mixture of solvent elution was adopted from previous research [26]. MIL-88(Fe) was regenerated by a simple process for 30 mins until the solution became completely clear. The reusability of MIL88B(Fe) was analyzed under the conditions of 50 mg L^{-1}, pH 9, and a contact time of 180 min. In this study, three-cycle experiments were conducted using regenerated MIL-88B(Fe), the effect of the regeneration cycle is depicted in Figure 7a. In comparison with fresh MIL-88B(Fe), the adsorption capacity on MB decreased by <10% at the second cycle, and after three cycles, the adsorbent capacity was reduced by 11.46 %, but remained at a high value (82.76%). This reveals an enhanced stability of MIL-88B(Fe) on MB adsorption. The adsorption capacity of MIL-88B(Fe) on RhB decreased by 10.37% from 82.76% to 72.41% in the second cycle and it decreased significantly from 72.41% to 41.47% in the third cycle. The results showed that the reusability of MIL-88B(Fe) towards MB adsorption was greater than RhB adsorption. The molecule size effect and bond strength between MIL-88B(Fe) and RhB may restrict the leaching process. The addition of strong acid such as HCl to the solvent may be required to remove RhB. According to the report in the literature, a high desorption efficiency of RhB-loaded Fe_3O_4/MIL-100(Fe) was accomplished using methanol as the solvent with the addition HCl (0.001 mol L-1). [45]. Nevertheless, it can be suggested that MIL-88B adsorption capacities towards both organic dyes are still good after regeneration, which indicates that the as-prepared MOF is completely recyclable.

Preprints (www.preprints.org) | NOT PEER-REVIEWED | Posted: 21 December 2023 doi:10.20944/preprints202312.1616.v1

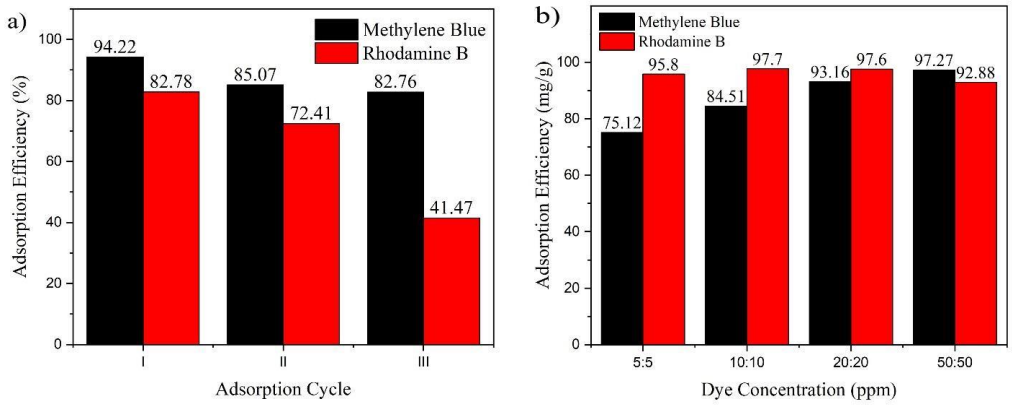

Figure 7. (a) Reusability and (b) adsorption capability of MIL-88B(Fe).

3.2.8. Selective Adsorption Capability

Another crucial aspect of the process of treating dye-wastewater was the selective adsorption of the particular dye. The experimental findings in Figure 7b demonstrate that competitive adsorption took place at low concentrations of both cationic dyes. Due to the interaction potency and breathing behavior of MIL-88B(Fe), RhB was more adsorbable than MB. However, at high concentrations, there is no discernible difference between MB and RhB adsorption. The interaction between the positive and negative charge of respective dyes and MIL-88B(Fe) which happen electrostatically affects the adsorption process. The anionic charge on MIL-88B(Fe) influences the adsorption selectivity of cationic dyes. It is evident that dyes in binary systems will not conflict with one another while adhering to MOF.

3.2.9. Comparison with Other Adsorbents

Table 5 summarizes the several studies on the adsorption of MB and RhB on porous solid materials reported by other research groups. As can be shown, MIL-88B(Fe) is an applicable adsorbent for the elimination of MB and RhB from aqueous solutions. Compared with other reported MOFs material and conventional adsorbents, the synthesized material has a medium BET surface area value and organic functional groups within the framework, which could be attractive for its rapidness and effective adsorption.

Table 5. Comparison of MB and RhB removal.

No	Adsorbent	BET Surface Area (m^2/g)	Adsorbate	Reaction Conditions					Ref
				C_0 (mg/L)	pH	Time (min)	Temp (°C)	Q_{max}* (mg/g)	
1	MIL-88B(Fe)	275.12	MB	250	9	180	25	162.82	This work
2	NH2-MIL-88B(Fe)	163.9	MB	20	3-11	45	35	61.46	[46]
3	MIL-101(Fe)	54.71	MB	200	9	500	25	58.82	[47]
4	Fe_3O_4 activated montmorillonite	147.92	MB	120-1000	7.37	25	20	106.38	[48,49]
5	MIL-88B(Fe)	275.12	RhB	250	9	180	25	144.65	This work
6	MIL-68(Al)	976	RhB	15	6.45	9.9	25	29.32	[50]
7	MIL-125(Ti)	845	RhB	10	7	180	25	59.92	[51]
8	Zirconium-based MOFs	-	RhB	10	7	240	25	67.73	[52]

[a] $q_{e,exp}$ is the equilibrium adsorption capacities in accordance to the experiments.

Preprints (www.preprints.org) | NOT PEER-REVIEWED | Posted: 21 December 2023 doi:10.20944/preprints202312.1616.v1

[b] $q_{e,cal}$ is determined in accordance to the linear fitting from the kinetic models.

3.2.10. Plausible Adsorption Mechanism

The dyes adsorption behavior in pH variations reflects the adsorption mechanism on the surface of MIL-88B(Fe). In basic pH, the adsorption capacity of MIL-88B(Fe) is higher than acid conditions for both dyes. Since MB and RhB are basic cationic dyes, they form cations (C^+) and reduced ions (CH^+) in water [53]. While the dyes possess a positive charge, the density of the negatively charged MIL-88B(Fe) increases in basic solution. The electrostatic interaction between oppositely charged (positive and negative) promotes the adsorption of dyes on the external area of MIL-88B(Fe). Binding is also ascribed to π-π interaction of the aromatic ring on MB and the MIL-88B(Fe) structure, whereas it does not form on RhB due to the steric hindrance [24,53]. The plausible adsorption mechanism is depicted in Figure 8.

Due to the surface-active sites, functional groups, and intraframework interactions that control on the flexibility of MIL-88B(Fe), the high adsorption capacity for both cationic dyes were made possible [54]. Firstly, the amount of –OH and C=O functional groups in MIL-88B(Fe) plays a crucial role in the adsorption process [24,55]. However, although MIL-88B(Fe) exhibits a larger adsorption capacity of MB in comparison to RhB, their adsorption does not compete with each other in a binary mixture (Figure 8). The high surface area of MIL-88B(Fe) leads to the high adsorption of a binary mixture of MB and RhB. Furthermore, the change in $\Delta G°$ value of RhB at T > 318 K confirms the flexibility of MIL-88B(Fe) framework, which is in line with report by Surble *et al.* The structure flexibility known as 'the breathing effect' is referred to the third-generation materials by Kitagawa [56,57]. Due to the bistable characteristic of MOFs under thermodynamic conditions (such as temperature, pressure, chemical inclusion, etc.), MOFs could exhibit breathable characteristics that could greatly expand their framework, showing their guest-induced feature [30,58]. Furthermore, after three cycles of regeneration, the adsorption capacity of MIL-88B(Fe) for MB remains high while that for RhB decreases. Based on the plausible mechanism in Figure 8, there is a chemical interaction between MIL-88B(Fe) and cationic dyes which is difficult to break by a simple washing method. Although it is quite effective to remove dyes using the simple solvent mixture, a more severe method is needed to separate dyes and MIL-88B(Fe). Therefore, this breathable feature of MIL-88B(Fe) is considered useful to overcome the pore size limitation often faced by adsorbents.

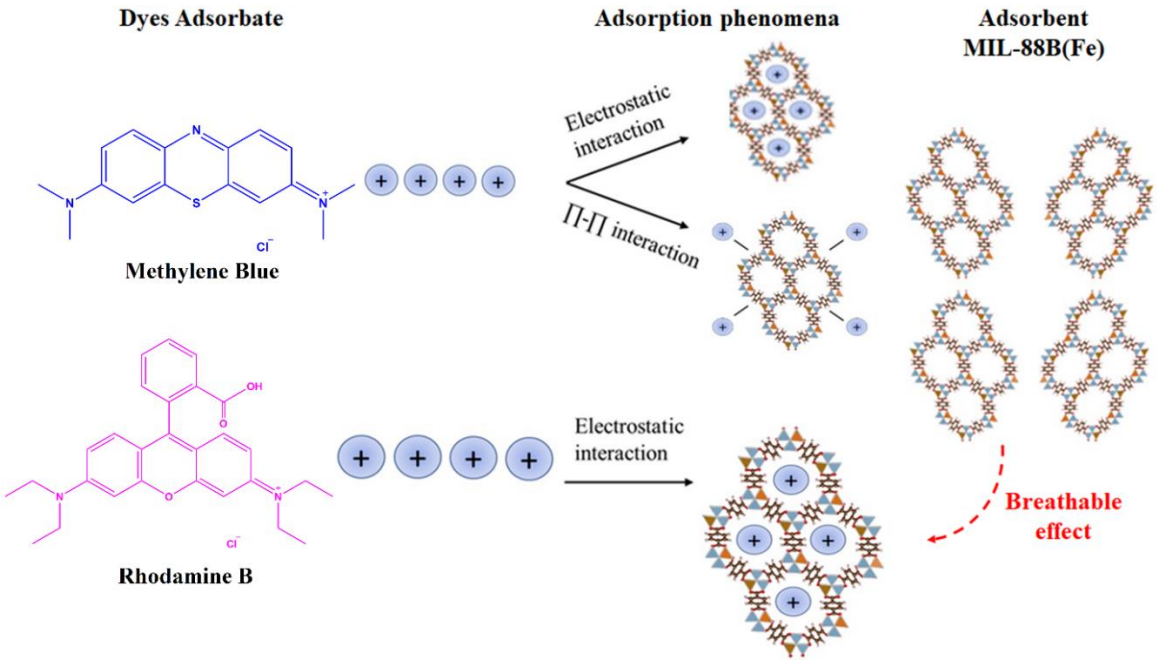

Figure 8. Plausible mechanism of MB and RhB dyes adsorption on the surface of MIL-88B(Fe).

4. Conclusions

The replacement of Cr^{3+} in MIL-101 by Fe^{3+} led to the creation of MIL-88B(Fe) adsorbent with good crystallinity and high surface area. MB adheres to MIL-88B(Fe) in accordance with the Langmuir model, which predicts one-layer chemisorption of the dyes on the MOF surface. On RhB, however, the Freundlich model performed better than the Langmuir model. Adsorption selectivity towards MB occurred in small concentrations of dyes mixture, while in larger concentrations, both MB and RhB can be adsorbed almost completely by MIL-88B (Fe) due to the breathing effect of the framework. The MIL-88B(Fe) can be reused as an effective adsorbent for removing MB and RhB after the third adsorption-desorption experiment. The capacity was slightly decreased towards methylene blue but significantly reduced when adsorbing RhB.

Supplementary Materials: The following supporting information can be downloaded at: www.mdpi.com/xxx/s1. The Rietveld refinement of XRD pattern, EDX spectrum, and N_2 physisorption graphs.

Author Contributions: Conceptualization, D.A.N. and Y.K.K.; methodology, D.A.N. and Y.K.K.; formal analysis, N.A., I.K., and Y.; investigation, N.A., I.K., and Y.; writing—original draft preparation, D.A.N. and N.A.; writing—review and editing, N.A., I.K., D.A.N., Y.K.K., and G.T.M.K.; supervision, D.A.N. and Y.K.K.; funding acquisition, Y.K.K. All authors have read and agreed to the published version of the manuscript.

Funding: This research was funded by Universitas Indonesia through Hibah Publikasi Terindeks Internasional (PUTI) Q2 Research Grant No. NKB-670/UN2.RST/HKP.05.00/2022 and the Indonesian Ministry of Research and Technology/ National Research and Innovation Agency (Menristek/BRIN) for funding the project with the BOPTN grant for Applied Research No. NKB-294/UN2.RST/HKP.05.00/2020.

Data Availability Statement: The data presented in this study are available upon request from the corresponding author and co-authors.

Conflicts of Interest: The authors declare no conflict of interest.

References

1. Karmakar, S.; Roy, D.; Janiak, C.; De, S. Insights into Multi-Component Adsorption of Reactive Dyes on MIL-101-Cr Metal Organic Framework: Experimental and Modeling Approach. *Sep Purif Technol* **2019**, *215*, 259–275, doi:10.1016/J.SEPPUR.2019.01.013.
2. Onu, C.E.; Asadu, C.O.; Ohale, P.E.; Ojukwu, E.V.; Ogunaobi, N.C.; Onu, C.P.; Akaeme, F.C. Recent Trends in Textile Wastewater Treatment Using Agricultural Waste. **2022**, 89–110, doi:10.1007/978-981-19-2852-9_6.
3. Ghasemi, H.; Aghabarari, B.; Alizadeh, M.; Khanlarkhani, A.; Abu-Zahra, N. High Efficiency Decolorization of Wastewater by Fenton Catalyst: Magnetic Iron-Copper Hybrid Oxides. *Journal of Water Process Engineering* **2020**, *37*, 101540, doi:10.1016/J.JWPE.2020.101540.
4. Chiu, Y.H.; Chang, T.F.M.; Chen, C.Y.; Sone, M.; Hsu, Y.J. Mechanistic Insights into Photodegradation of Organic Dyes Using Heterostructure Photocatalysts. *Catalysts 2019, Vol. 9, Page 430* **2019**, *9*, 430, doi:10.3390/CATAL9050430.
5. Demissie, H.; An, G.; Jiao, R.; Ritigala, T.; Lu, S.; Wang, D. Modification of High Content Nanocluster-Based Coagulation for Rapid Removal of Dye from Water and the Mechanism. *Sep Purif Technol* **2021**, *259*, 117845, doi:10.1016/J.SEPPUR.2020.117845.
6. Zazou, H.; Afanga, H.; Akhouairi, S.; Ouchtak, H.; Addi, A.A.; Akbour, R.A.; Assabbane, A.; Douch, J.; Elmchaouri, A.; Duplay, J.; et al. Treatment of Textile Industry Wastewater by Electrocoagulation Coupled with Electrochemical Advanced Oxidation Process. *Journal of Water Process Engineering* **2019**, *28*, 214–221, doi:10.1016/J.JWPE.2019.02.006.
7. Zhu, T.T.; Zhang, Z.M.; Chen, W.L.; Liu, Z.J.; Wang, E.B. Encapsulation of Tungstophosphoric Acid into Harmless MIL-101(Fe) for Effectively Removing Cationic Dye from Aqueous Solution. *RSC Adv* **2016**, *6*, 81622–81630, doi:10.1039/C6RA16716K.
8. Adeyemo, A.A.; Adeoye, I.O.; Bello, O.S. Metal Organic Frameworks as Adsorbents for Dye Adsorption: Overview, Prospects and Future Challenges. *https://doi.org/10.1080/02772248.2012.744023* **2012**, *94*, 1846–1863, doi:10.1080/02772248.2012.744023.
9. Haque, E.; Jun, J.W.; Jhung, S.H. Adsorptive Removal of Methyl Orange and Methylene Blue from Aqueous Solution with a Metal-Organic Framework Material, Iron Terephthalate (MOF-235). *J Hazard Mater* **2011**, *185*, 507–511, doi:10.1016/J.JHAZMAT.2010.09.035.
10. Lin, S.; Song, Z.; Che, G.; Ren, A.; Li, P.; Liu, C.; Zhang, J. Adsorption Behavior of Metal–Organic Frameworks for Methylene Blue from Aqueous Solution. *Microporous and Mesoporous Materials* **2014**, *193*, 27–34, doi:10.1016/J.MICROMESO.2014.03.004.

11. Wu, Z.; Chen, C.; Wan, H.; Wang, L.; Li, Z.; Li, B.; Guo, Q.; Guan, G. Fabrication of Magnetic NH2-MIL-88B (Fe) Confined Brønsted Ionic Liquid as an Efficient Catalyst in Biodiesel Synthesis. *Energy and Fuels* **2016**, *30*, 10739–10746, doi:10.1021/ACS.ENERGYFUELS.6B01212.
12. Zhu, G.; Xing, X.; Wang, J.; Zhang, X. Effect of Acid and Hydrothermal Treatments on the Dye Adsorption Properties of Biomass-Derived Activated Carbon. *J Mater Sci* **2017**, *52*, 7664–7676, doi:10.1007/S10853-017-1055-0/TABLES/4.
13. Shafqat, S.R.; Bhawani, S.A.; Bakhtiar, S.; Ibrahim, M.N.M. Synthesis of Molecularly Imprinted Polymer for Removal of Congo Red. *BMC Chem* **2020**, *14*, 1–15, doi:10.1186/S13065-020-00680-8/TABLES/6.
14. Rahimi, B.; Jafari, N.; Abdolahnejad, A.; Farrokhzadeh, H.; Ebrahimi, A. Application of Efficient Photocatalytic Process Using a Novel BiVO/TiO2-NaY Zeolite Composite for Removal of Acid Orange 10 Dye in Aqueous Solutions: Modeling by Response Surface Methodology (RSM). *J Environ Chem Eng* **2019**, *7*, 103253, doi:10.1016/J.JECE.2019.103253.
15. Zango, Z.U.; Jumbri, K.; Sambudi, N.S.; Hanif Abu Bakar, N.H.; Fathihah Abdullah, N.A.; Basheer, C.; Saad, B. Removal of Anthracene in Water by MIL-88(Fe), NH 2 -MIL-88(Fe), and Mixed-MIL-88(Fe) Metal–Organic Frameworks. *RSC Adv* **2019**, *9*, 41490–41501, doi:10.1039/C9RA08660A.
16. James, S.L. Metal-Organic Frameworks. *Chem Soc Rev* **2003**, *32*, 276–288, doi:10.1039/B200393G.
17. Britt, D.; Tranchemontagne, D.; Yaghi, O.M. Metal-Organic Frameworks with High Capacity and Selectivity for Harmful Gases. *Proc Natl Acad Sci U S A* **2008**, *105*, 11623–11627, doi:10.1073/PNAS.0804900105/SUPPL_FILE/0804900105SI.PDF.
18. Liu, X.; Zhou, Y.; Zhang, J.; Tang, L.; Luo, L.; Zeng, G. Iron Containing Metal-Organic Frameworks: Structure, Synthesis, and Applications in Environmental Remediation. *ACS Appl Mater Interfaces* **2017**, *9*, 20255–20275, doi:10.1021/ACSAMI.7B02563/ASSET/IMAGES/MEDIUM/AM-2017-02563E_0022.GIF.
19. Li, C.; Xiong, Z.; Zhang, J.; Wu, C. The Strengthening Role of the Amino Group in Metal-Organic Framework MIL-53 (Al) for Methylene Blue and Malachite Green Dye Adsorption. *J Chem Eng Data* **2015**, *60*, 3414–3422, doi:10.1021/ACS.JCED.5B00692/SUPPL_FILE/JE5B00692_SI_001.PDF.
20. Fu, Q.; Lou, J.; Zhang, R.; Peng, L.; Zhou, S.; Yan, W.; Mo, C.; Luo, J. Highly Effective and Fast Removal of Congo Red from Wastewater with Metal-Organic Framework Fe-MIL-88NH2. *J Solid State Chem* **2021**, *294*, 121836, doi:10.1016/J.JSSC.2020.121836.
21. Uddin, M.J.; Ampiaw, R.E.; Lee, W. Adsorptive Removal of Dyes from Wastewater Using a Metal-Organic Framework: A Review. *Chemosphere* **2021**, *284*, 131314, doi:10.1016/J.CHEMOSPHERE.2021.131314.
22. Abbasi, A.R.; Karimi, M.; Daasbjerg, K. Efficient Removal of Crystal Violet and Methylene Blue from Wastewater by Ultrasound Nanoparticles Cu-MOF in Comparison with Mechanosynthesis Method. *Ultrason Sonochem* **2017**, *37*, 182–191, doi:10.1016/J.ULTSONCH.2017.01.007.
23. Zhang, J.; Li, F.; Sun, Q. Rapid and Selective Adsorption of Cationic Dyes by a Unique Metal-Organic Framework with Decorated Pore Surface. *Appl Surf Sci* **2018**, *440*, 1219–1226, doi:10.1016/J.APSUSC.2018.01.258.
24. Ghosh, A.; Das, G. Green Synthesis of Sn(II)-BDC MOF: Preferential and Efficient Adsorption of Anionic Dyes. *Microporous and Mesoporous Materials* **2020**, *297*, 110039, doi:10.1016/J.MICROMESO.2020.110039.
25. Agustin, M.; Nurani, D.A.; Zulys, A.; Krisnandi, Y.K. Adsorption of Rhodamine B by Yttrium-Succinate Metal Organic Framework (MOF). *AIP Conf Proc* **2020**, *2243*, 030001, doi:10.1063/5.0001094.
26. Nurani, D.A.; Butar, B.C.B.; Krisnandi, Y.K. Synthesis and Characterization of Metal Organic Framework Using Succinic Acid Ligand with Cobalt and Iron Metals as Methylene Blue Dye Adsorbent. *IOP Conf Ser Mater Sci Eng* **2020**, *902*, 012055, doi:10.1088/1757-899X/902/1/012055.
27. Knyazeva, M.K.; Shkolin, A. V.; Fomkin, A.A.; Tsivadze, A.Y.; Solovtsova, O. V.; Platonova, N.P.; Pulin, A.L.; Men'shchikov, I.E.; Shiryaev, A.A.; Vysotskii, V. V.; et al. Synthesis and Structural-Energy Characteristics of Fe-BDC Metal-Organic Frameworks. *Protection of Metals and Physical Chemistry of Surfaces* **2018**, *54*, 1004–1009, doi:10.1134/S2070205118060151/TABLES/5.
28. Pertiwi, R.; Oozeerally, R.; Burnett, D.L.; Chamberlain, T.W.; Cherkasov, N.; Walker, M.; Kashtiban, R.J.; Krisnandi, Y.K.; Degirmenci, V.; Walton, R.I. Replacement of Chromium by Non-Toxic Metals in Lewis-Acid MOFs: Assessment of Stability as Glucose Conversion Catalysts. *Catalysts 2019, Vol. 9, Page 437* **2019**, *9*, 437, doi:10.3390/CATAL9050437.
29. Wu, L.; Chaplais, G.; Xue, M.; Qiu, S.; Patarin, J.; Simon-Masseron, A.; Chen, H. New Functionalized MIL-53(In) Solids: Syntheses, Characterization, Sorption, and Structural Flexibility. *RSC Adv* **2019**, *9*, 1918–1928, doi:10.1039/C8RA08522F.
30. Wei, Y.S.; Chen, K.J.; Liao, P.Q.; Zhu, B.Y.; Lin, R.B.; Zhou, H.L.; Wang, B.Y.; Xue, W.; Zhang, J.P.; Chen, X.M. Turning on the Flexibility of Isoreticular Porous Coordination Frameworks for Drastically Tunable Framework Breathing and Thermal Expansion. *Chem Sci* **2013**, *4*, 1539–1546, doi:10.1039/C3SC22222E.
31. Chaplais, G.; Simon-Masseron, A.; Porcher, F.; Lecomte, C.; Bazer-Bachi, D.; Bats, N.; Patarin, J. IM-19: A New Flexible Microporous Gallium Based-MOF Framework with Pressure- and Temperature-Dependent Openings. *Physical Chemistry Chemical Physics* **2009**, *11*, 5241–5245, doi:10.1039/B822163D.

32. Volkringer, C.; Loiseau, T.; Guillou, N.; Férey, G.; Elkaïm, E.; Vimont, A. XRD and IR Structural Investigations of a Particular Breathing Effect in the MOF-Type Gallium Terephthalate MIL-53(Ga). *Dalton Transactions* **2009**, 2241–2249, doi:10.1039/B817563B.
33. Surblé, S.; Serre, C.; Mellot-Draznieks, C.; Millange, F.; Férey, G. A New Isoreticular Class of Metal-Organic-Frameworks with the MIL-88 Topology. *Chemical Communications* **2006**, 284–286, doi:10.1039/B512169H.
34. Toby, B.H. R Factors in Rietveld Analysis: How Good Is Good Enough? *Powder Diffr* **2006**, *21*, 67–70, doi:10.1154/1.2179804.
35. Carson, F.; Su, J.; Platero-Prats, A.E.; Wan, W.; Yun, Y.; Samain, L.; Zou, X. Framework Isomerism in Vanadium Metal-Organic Frameworks: MIL-88B(V) and MIL-101(V). *Cryst Growth Des* **2013**, *13*, 5036–5044, doi:10.1021/CG4012058/SUPPL_FILE/CG4012058_SI_001.PDF.
36. Taylor-Pashow, K.M.L.; Della Rocca, J.; Xie, Z.; Tran, S.; Lin, W. Postsynthetic Modifications of Iron-Carboxylate Nanoscale Metal-Organic Frameworks for Imaging and Drug Delivery. *J Am Chem Soc* **2009**, *131*, 14261–14263, doi:10.1021/JA906198Y/SUPPL_FILE/JA906198Y_SI_001.PDF.
37. Hidalgo, T.; Alonso-Nocelo, M.; Bouzo, B.L.; Reimondez-Troitiño, S.; Abuin-Redondo, C.; De La Fuente, M.; Horcajada, P. Biocompatible Iron(III) Carboxylate Metal–Organic Frameworks as Promising RNA Nanocarriers. *Nanoscale* **2020**, *12*, 4839–4845, doi:10.1039/C9NR08127E.
38. Revellame, E.D.; Fortela, D.L.; Sharp, W.; Hernandez, R.; Zappi, M.E. Adsorption Kinetic Modeling Using Pseudo-First Order and Pseudo-Second Order Rate Laws: A Review. *Clean Eng Technol* **2020**, *1*, 100032, doi:10.1016/J.CLET.2020.100032.
39. Zhang, G.; Wo, R.; Sun, Z.; Hao, G.; Liu, G.; Zhang, Y.; Guo, H.; Jiang, W. Effective Magnetic Mofs Adsorbent for the Removal of Bisphenol a, Tetracycline, Congo Red and Methylene Blue Pollutions. *Nanomaterials* **2021**, *11*, 1917, doi:10.3390/NANO11081917/S1.
40. Wang, X.; Jiang, C.; Hou, B.; Wang, Y.; Hao, C.; Wu, J. Carbon Composite Lignin-Based Adsorbents for the Adsorption of Dyes. *Chemosphere* **2018**, *206*, 587–596, doi:10.1016/J.CHEMOSPHERE.2018.04.183.
41. Yadav, M.; Thakore, S.; Jadeja, R. Removal of Organic Dyes Using Fucus Vesiculosus Seaweed Bioadsorbent an Ecofriendly Approach: Equilibrium, Kinetics and Thermodynamic Studies. *Environmental Chemistry and Ecotoxicology* **2022**, *4*, 67–77, doi:10.1016/J.ENCECO.2021.12.003.
42. Kundu, A.; Mondal, A. Kinetics, Isotherm, and Thermodynamic Studies of Methylene Blue Selective Adsorption and Photocatalysis of Malachite Green from Aqueous Solution Using Layered Na-Intercalated Cu-Doped Titania. *Appl Clay Sci* **2019**, *183*, 105323, doi:10.1016/J.CLAY.2019.105323.
43. Konicki, W.; Hełminiak, A.; Arabczyk, W.; Mijowska, E. Adsorption of Cationic Dyes onto Fe@graphite Core–Shell Magnetic Nanocomposite: Equilibrium, Kinetics and Thermodynamics. *Chemical Engineering Research and Design* **2018**, *129*, 259–270, doi:10.1016/J.CHERD.2017.11.004.
44. Feng, M.; Yu, S.; Wu, P.; Wang, Z.; Liu, S.; Fu, J. Rapid, High-Efficient and Selective Removal of Cationic Dyes from Wastewater Using Hollow Polydopamine Microcapsules: Isotherm, Kinetics, Thermodynamics and Mechanism. *Appl Surf Sci* **2021**, *542*, 148633, doi:10.1016/J.APSUSC.2020.148633.
45. Liu, H.; Ren, X.; Chen, L. Synthesis and Characterization of Magnetic Metal–Organic Framework for the Adsorptive Removal of Rhodamine B from Aqueous Solution. *Journal of Industrial and Engineering Chemistry* **2016**, *34*, 278–285, doi:10.1016/J.JIEC.2015.11.020.
46. He, J.; Zhang, Y.; Zhang, X.; Huang, Y. Highly Efficient Fenton and Enzyme-Mimetic Activities of NH2-MIL-88B(Fe) Metal Organic Framework for Methylene Blue Degradation. *Scientific Reports 2018 8:1* **2018**, *8*, 1–8, doi:10.1038/s41598-018-23557-2.
47. Eltaweil, A.S.; Abd El-Monaem, E.M.; Omer, A.M.; Khalifa, R.E.; Abd El-Latif, M.M.; El-Subruiti, G.M.; Omer, A.M. Efficient Removal of Toxic Methylene Blue (MB) Dye from Aqueous Solution Using a Metal-Organic Framework (MOF) MIL-101(Fe): Isotherms, Kinetics, and Thermodynamic Studies. **2020**, doi:10.5004/dwt.2020.25599.
48. Chang, J.; Ma, J.; Ma, Q.; Zhang, D.; Qiao, N.; Hu, M.; Ma, H. Adsorption of Methylene Blue onto Fe3O4/Activated Montmorillonite Nanocomposite. *Appl Clay Sci* **2016**, *119*, 132–140, doi:10.1016/J.CLAY.2015.06.038.
49. Mashkoor, F.; Nasar, A. Magsorbents: Potential Candidates in Wastewater Treatment Technology – A Review on the Removal of Methylene Blue Dye. *J Magn Magn Mater* **2020**, *500*, 166408, doi:10.1016/J.JMMM.2020.166408.
50. Saghanejhad Tehrani, M.; Zare-Dorabei, R. Highly Efficient Simultaneous Ultrasonic-Assisted Adsorption of Methylene Blue and Rhodamine B onto Metal Organic Framework MIL-68(Al): Central Composite Design Optimization. *RSC Adv* **2016**, *6*, 27416–27425, doi:10.1039/C5RA28052D.
51. Guo, H.; Lin, F.; Chen, J.; Li, F.; Weng, W. Metal–Organic Framework MIL-125(Ti) for Efficient Adsorptive Removal of Rhodamine B from Aqueous Solution. *Appl Organomet Chem* **2015**, *29*, 12–19, doi:10.1002/AOC.3237.
52. Zhao, J.; Xu, L.; Su, Y.; Yu, H.; Liu, H.; Qian, S.; Zheng, W.; Zhao, Y. Zr-MOFs Loaded on Polyurethane Foam by Polydopamine for Enhanced Dye Adsorption. *Journal of Environmental Sciences* **2021**, *101*, 177–188, doi:10.1016/J.JES.2020.08.021.

53. Arora, C.; Soni, S.; Sahu, S.; Mittal, J.; Kumar, P.; Bajpai, P.K. Iron Based Metal Organic Framework for Efficient Removal of Methylene Blue Dye from Industrial Waste. *J Mol Liq* **2019**, *284*, 343–352, doi:10.1016/J.MOLLIQ.2019.04.012.
54. Yilmaz, E.; Sert, E.; Atalay, F.S. Synthesis, Characterization of a Metal Organic Framework: MIL-53 (Fe) and Adsorption Mechanisms of Methyl Red onto MIL-53 (Fe). *J Taiwan Inst Chem Eng* **2016**, *65*, 323–330, doi:10.1016/J.JTICE.2016.05.028.
55. Devic, T.; Horcajada, P.; Serre, C.; Salles, F.; Maurin, G.; Moulin, B.; Heurtaux, D.; Clet, G.; Vimont, A.; Grenéche, J.M.; et al. Functionalization in Flexible Porous Solids: Effects on the Pore Opening and the Host-Guest Interactions. *J Am Chem Soc* **2010**, *132*, 1127–1136, doi:10.1021/JA9092715/SUPPL_FILE/JA9092715_SI_004.PDF.
56. Uemura, K.; Matsuda, R.; Kitagawa, S. Flexible Microporous Coordination Polymers. *J Solid State Chem* **2005**, *178*, 2420–2429, doi:10.1016/J.JSSC.2005.05.036.
57. Fletcher, A.J.; Thomas, K.M.; Rosseinsky, M.J. Flexibility in Metal-Organic Framework Materials: Impact on Sorption Properties. *J Solid State Chem* **2005**, *178*, 2491–2510, doi:10.1016/J.JSSC.2005.05.019.
58. Long, J.; Yaghi, O.; Ge´rard, G.; Fe´rey, F.; Serre, C. Large Breathing Effects in Three-Dimensional Porous Hybrid Matter: Facts, Analyses, Rules and Consequences. *Chem Soc Rev* **2009**, *38*, 1380–1399, doi:10.1039/B804302G.